Combined Operando UV/Vis/IR Spectroscopy Reveals the Role of Methoxy and Aromatic Species during the Methanol-to-Olefins Reaction over H-SAPO-34

Qingyun Qian,[a] Charlotte Vogt,[a] Mohamed Mokhtar,[b] Abdullah M. Asiri,[b] Shaeel A. Al-Thabaiti,[b] Suliman N. Basahel,[b] Javier Ruiz-Martínez,*[a] and Bert M. Weckhuysen*[a]

The methanol-to-olefins (MTO) process over H-SAPO-34 is investigated by using an operando approach combining UV/Vis and IR spectroscopies with on-line mass spectrometry. Methanol, methoxy, and protonated dimethyl ether are the major species during the induction period, whereas polyalkylated benzenes and polyaromatic species are encountered in the active stage of the MTO process. The accessibility of SAPO-34 is linked with the amount of methoxy species, whereas the formation of polyaromatic species that block the pores is the main cause of deactivation. Furthermore, the reaction pathways responsible for the formation of olefins and polyaromatics co-exist and compete during the whole MTO process, and both routes are directly related to the amount of surface polyalkylated benzene carbocations and methoxy species. Hence, a first-order kinetic model is proposed and comparable activation energies for both processes are obtained.

Introduction

The increase in energy demand and dwindling resources of crude oil are stimulating scientists to pursue more efficient processes and examine the use of alternative feedstocks, such as coal, natural gas, and biomass, for the production of fuels and chemicals. One of the promising technologies is the conversion of these feedstocks to methanol by syngas synthesis[1] and subsequent synthesis of light olefins and gasoline-range hydrocarbons by the methanol-to-hydrocarbons (MTH) process by using Brønsted acid zeolites.[2] Since the MTH was discovered by serendipity in 1976–77,[3] intensive research has yielded many advances in the understanding of the reaction mechanism and related catalyst deactivation. In H-ZSM-5 and H-SAPO-34, two of the archetypal MTH catalysts, the reaction is believed to occur through the hydrocarbon pool mechanism, in which polymethyl-substituted benzene molecules are the active species.[4] These methylated benzene species produce olefins by splitting off alkyl groups. The chemistry involved in the reaction mechanism is under intensive study by theoretical[5] and experimental analytical approaches ranging isotopic labeling,[6] chromatography,[7] mass spectrometry,[8] and several spectroscopic[4c, 9] methods. Another important aspect in the MTH chemistry is to understand the mechanism and kinetics involved during the deactivation of the zeolite catalyst. It is believed that coke deposition is the main cause of deactivation. Several properties of the material, such as crystal size, acid strength, and acid site density play a key role in the deactivation mechanism by coke deposition.[10] Although reaction conditions may play a role, the topology of the zeotype controls mainly the nature and location of the coke species that deactivate the catalyst. For instance, in zeolite MFI structures, such as ZSM-5, deposition of highly conjugated polyaromatic (PA) species on the external surface of the material appears to be the main reason for catalyst deactivation.[11] In the case of chabazite topology, formation of less-extended polyaromatics that fill the nanocages of the structure is believed to be the reason for the loss of catalytic activity and subsequent deactivation.[12]

Despite the efforts made to elucidate the deactivation mechanism, knowledge of the detailed chemistry behind the species deactivating the catalyst is still limited. This is due to the lack of studies integrating two main measurements: Firstly, the combination of spectroscopic techniques that provide complementary information to give insight into the nature of those species under real reaction conditions. Secondly, the measurement of the catalytic performance during the collection of spectroscopic information. The combination of spectroscopic approaches has been successfully applied in several catalytic systems, as detailed in a recent review.[13]

In this paper we superimpose both approaches with the goal of identifying the active and deactivating species in the MTO process on H-SAPO-34. To achieve this goal, we use an innovative methodology combining operando UV/Vis spectroscopy, IR spectroscopy, and on-line catalytic activity measurements. In such an approach, the spectroscopic information is

[a] Dr. Q. Qian, C. Vogt, Dr. J. Ruiz-Martínez, Prof. Dr. B. M. Weckhuysen
Inorganic Chemistry and Catalysis group
Debye Institute for Nanomaterials Science
Utrecht University
Universiteitsweg 99, 3584 CG Utrecht (The Netherlands)
E-mail: b.m.weckhuysen@uu.nl
        j.ruizmartinez@uu.nl

[b] Dr. M. Mokhtar, Prof. Dr. A. M. Asiri, Prof. Dr. S. A. Al-Thabaiti, Prof. Dr. S. N. Basahel
Department of Chemistry
Faculty of Science King Abdulaziz University
P.O. Box 80203, 21589 Jeddah (Saudi Arabia)

Supporting information for this article is available on the WWW under http://dx.doi.org/10.1002/cctc.201402714.

collected at the same spot on the catalyst sample and correlated with the catalytic activity of the material, as displayed in Figure S1. Based on the catalytic and spectroscopic information obtained, the formation of olefins and PA species is discussed.

Results and Discussion

The physicochemical properties of the H-SAPO-34 catalyst material under study have been reported in the previous work of our group.[14] Nitrogen physisorption results indicated that the H-SAPO-34 sample is mainly microporous with a BET surface area of 594 $m^2 g^{-1}$ and a micropore volume of 0.22 $cm^3 g^{-1}$. X-ray diffraction measurements showed a typical pattern of the chabazite framework structure and no signs of other impurity phases were observed. The ammonia TPD profile of the H-SAPO-34 evidenced a combination of both strong and weak acid sites characteristic of H-SAPO-34 materials.

Revealing reaction intermediates and deactivating species

In a first set of experiments, we studied the H-SAPO-34 system by performing a temperature-programmed methanol-to-olefins (MTO) reaction and followed the activity by using on-line mass spectrometry. The catalytic performance during the reaction is shown in Figure 1, in which for the sake of clarity only methanol, dimethyl ether (DME) and propylene are represented. DME originates from the dehydration of methanol and is not considered a desired product of the MTO reaction. Propylene is a representative product during the MTO reaction on H-SAPO-34 and we monitor it to evaluate the catalytic performance of the material. By examining the propylene profile, three main regions can be distinguished: 1) the induction period, below 573 K, in which no propylene is formed and only dehydration of methanol into DME occurs; 2) the reaction period, at 583–653 K, in which the catalyst is functioning in the MTO reaction; and 3) the deactivation period, in which the formation of propylene drops and the catalyst is deactivated completely from 653 K onwards.
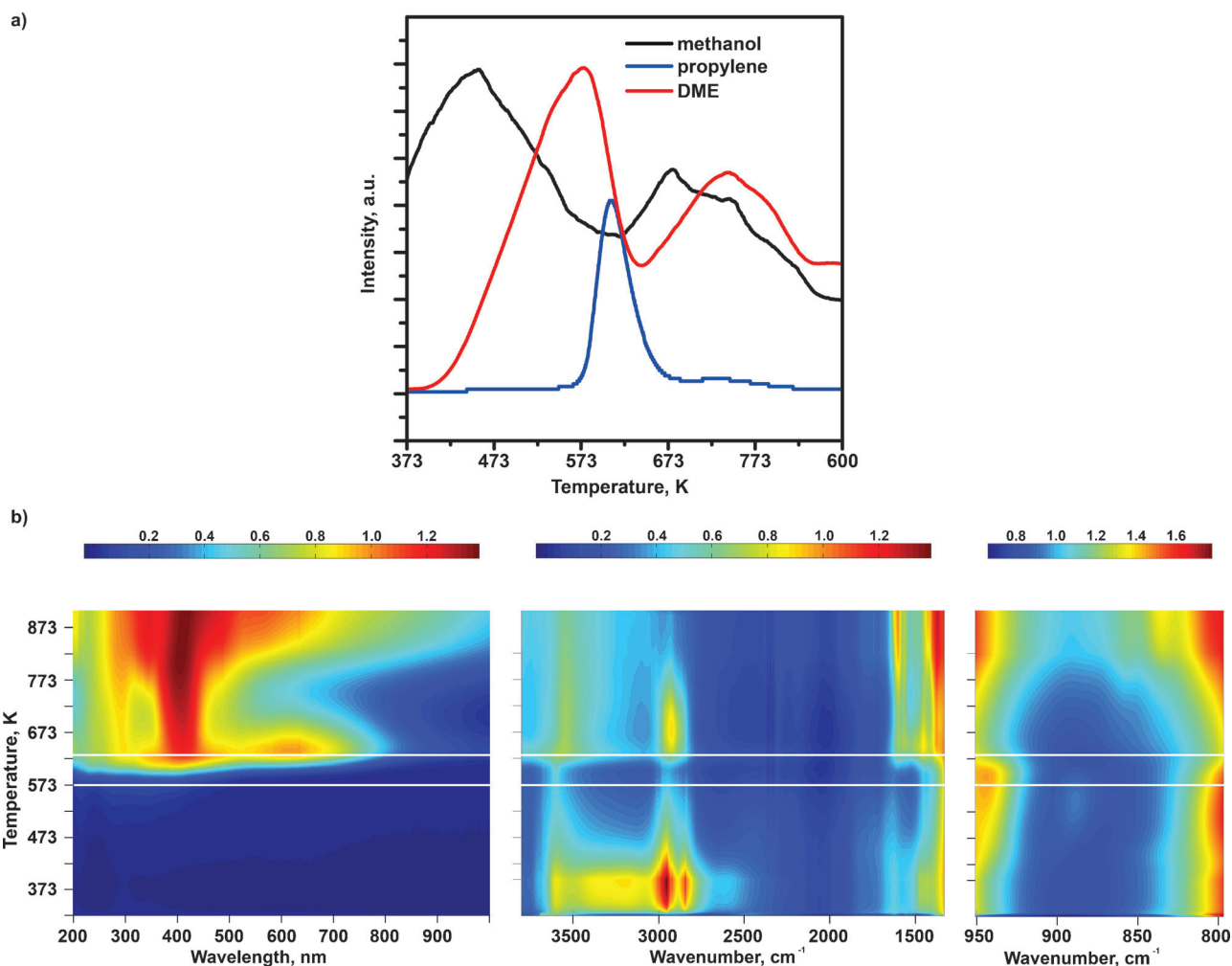

Figure 1. a) Catalytic performance of the H-SAPO-34 catalyst during the temperature-programmed MTO reaction. Reaction products were identified by on-line mass spectrometry. b) Overall spectroscopic information in color-coded graphs acquired from the catalyst wafer by combining operando UV/Vis (left) and IR (middle and right) spectroscopy. The three main regions of the temperature-programmed reaction are separated by horizontal white lines.

2

These are not the final page numbers! ↗↗

By investigation of the catalytic properties of the material, we aim for an analysis of the species formed on the catalyst wafer during the different stages of the catalytic reaction. The operando UV/Vis and IR spectroscopic results summarized in Figure 1 b reveal changes in the spectra during the different stages, which are separated by white lines. In view of the complexity and dynamics of the spectra, we have decided to inspect and discuss the different stages of the reaction separately. In addition, for a better evaluation of each catalytic stage, the spectra discussed and plotted in this work include a spectrum or spectra from the previous and/or subsequent catalytic step(s). A number of operando UV/Vis spectra of the catalyst during the induction period are shown in Figure 2 a. The spec-

H-SAPO-34 zeotypes. The low absorbance of these bands suggests that these species are most likely formed by the presence of impurities in the methanol feed. It is known that small amounts of ethanol, propanol, or acetaldehyde can always be found in methanol, thus, these impurities might form the first aromatics. Another plausible explanation for the formation of such species is the interaction of methanol with organic residues from the detemplation step.[18]

Due to the low formation of olefinic and aromatic species, as monitored by UV/Vis spectroscopy, we aim to study other species that might be spectroscopically silent in the UV/Vis region. With this in mind, we have evaluated the operando IR spectra of the catalyst wafer and several representative IR spectra are depicted in Figure 2 b. The IR spectrum of the catalyst before reaction shows three main peaks in the OH stretching region ($\tilde{\nu} =$ 3600 cm^{-1}). The peaks at $\tilde{\nu} =$ 3625 and 3595 cm^{-1} are the high and low frequency OH stretching signatures of the Brønsted acid sites, whereas the one at $\tilde{\nu} = 3675$ cm^{-1} is ascribed to phosphorus hydroxyl groups,[19] most likely coming from the external surface of the zeotype crystals. On flowing methanol through the catalyst at 393 K, the intensity of the band in the OH region clearly decreases and the band broadens. The former can be ascribed to a loss of Brønsted acidity and the latter to the nearly free OH stretching mode of methanol.[20] At $\tilde{\nu} \approx 3000$ cm^{-1}, several bands arise, predominantly two at $\tilde{\nu} = 2950$ and 2845 cm^{-1}, which are CH stretching vibrations attributable to methanol physically adsorbed on the catalyst wafer.[20] On increasing the reaction temperature, the shape and intensity of the CH stretching region evolve,
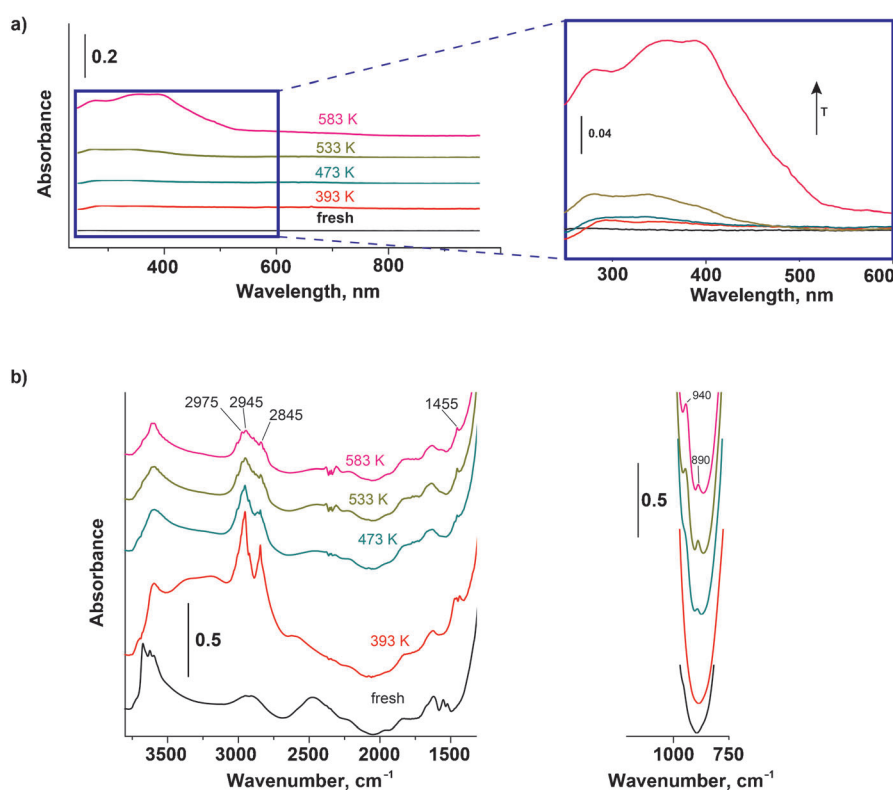

Figure 2. Spectroscopic information for the H-SAPO-34 catalyst wafer during the induction period of the temperature-programmed MTO reaction: a) Operando UV/Vis spectra at different reaction temperatures. Insert: Zoom-in of the non-stacked spectra. b) Operando IR spectra at different reaction temperatures. The operando UV/Vis and IR spectra are stacked for clarity.

tra display a lack of absorbance in the UV/Vis region during this period, and only at the beginning of the reaction, which starts at approximately 573 K, is a low absorbance observed as can be seen in the spectra at 583 K. A magnification of the spectra, shown in Figure 2 a (right), allows us to perceive distinct weak bands in the UV region of the spectra (at $\lambda <$ 400 nm). Three main absorption bands can be detected: one at $\lambda = 270$ nm, corresponding to neutral benzene species,[10d, 15] another at $\lambda = 345$ nm, which is ascribed to dienyl carbenium ions,[10d, 16] and an absorption band at $\lambda \approx 390$ nm due to poly-alkylated benzene (PAB) carbocations,[7b, 16, 17] which are believed to be the main catalytic engine in the MTO reaction on

which reflects a change in the chemistry of the species. The bands ascribed to physisorbed methanol diminish and a new set of bands appears. More specifically, the band at $\tilde{\nu} = 2975$ cm^{-1} can be ascribed to the CH stretching from methoxy species on Brønsted acid sites.[21] The existence of methoxy species can be confirmed by the presence of a methyl asymmetric bending band of such species at $\tilde{\nu} = 1455$ cm^{-1}.[21c] The three bands at $\tilde{\nu} = 3010$, 2945, and 2845 cm^{-1} are typical methyl asymmetric and symmetric stretching modes from DME protonated on Brønsted acid sites.[21b] If we now look to the low frequency region, two bands appear at $\tilde{\nu} = 940$ and 890 cm^{-1} that are most likely the CO stretching modes of me-

These are not the final page numbers! ↗↗

thoxy and protonated DME on the catalysts. In conclusion, in the induction period the main hydrocarbon species adsorbed on the SAPO-34 are methanol, methoxy, and protonated DME, and small traces of olefins and aromatics.

In the next step, we aim to understand the chemistry of the species formed on the catalysts during the reaction period in the temperature region 583–653 K. From the activity data, two main regimes can be distinguished: the first one up to 623 K in which the amount of propylene increases with time on stream and the second one in which the propylene formation decreases. From inspection of the operando UV/Vis spectra collected during this period, displayed in Figure 3 a, one can clearly see a strong increase in the absorbance with the reaction temperature. This implies that the new species formed are essential for the production of olefins. At temperatures below 623 K, the intensity of the bands at $\lambda = 275$ and 390 nm, ascribed respectively to neutral and protonated methyl benzenes, grows with time on stream and indicates the formation of the active species during the reaction. In addition, both bands shift to higher wavelengths with the reaction temperature during this period. The band shift from $\lambda = 275$ nm to 295 nm could owe to the formation of monoenylic carbocations,[16] which can be an indication of olefin formation. Mono-

enylic species are allylic carbocations and can be formed by protonation of olefins on a Brønsted acid site and subsequent hydride abstraction.[22] The band shift from $\lambda = 390$ nm to 413 nm is ascribed to the formation of more alkylated benzene carbocations, methylated naphthalene carbocations, or PA neutral species.[10d,23] Interestingly, the band ascribed to the dienyl carbocationic species ($\lambda = 345$ nm) also increases during the active period of the material, but the exact nature and role of such species during the reaction still remain unclear. We contemplate two main hypotheses: 1) The dienyl carbocations are aromatic precursors originating from methylation and/or oligomerization of light olefins; however, as these species already form in the induction period, their olefinic origin is very unlikely. 2) The dienyl carbocations are reaction intermediates in the formation of light olefins; in this line of thinking, they could be cyclopentadienyl cations or less-methylated benzene carbocations. Additionally, in the high wavelength region, a band appears at $\lambda \approx 600$ nm, which according to previous theoretical studies can be ascribed to highly methylated PA carbocations, such as highly methylated naphthalene or phenanthrene-like species.[23]

At temperatures above 623 K, the catalyst starts to deactivate and this is reflected in the evolution of several bands.
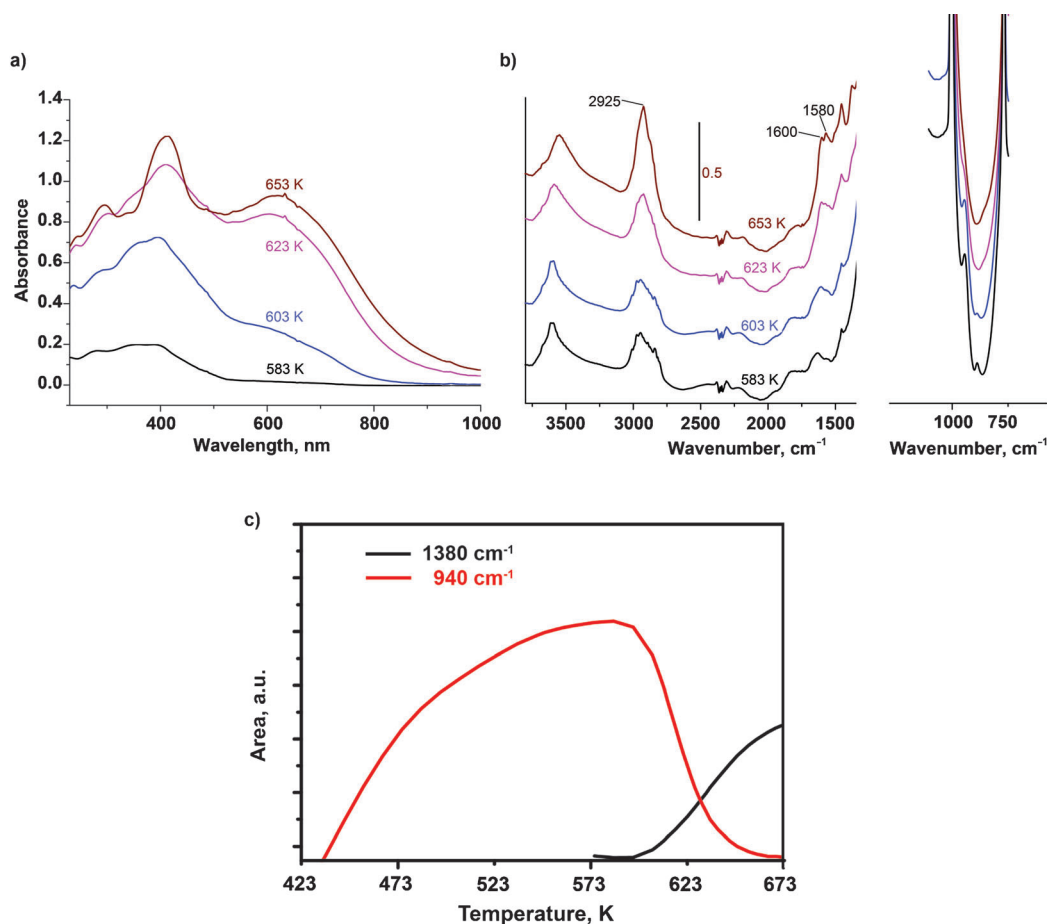

Figure 3. Spectroscopic information of the H-SAPO-34 catalyst during the reaction period of the temperature-programmed MTO reaction: a) Operando UV/Vis and b) Operando IR spectra. c) Integrated area of the $\tilde{\nu} = 1380$ and 940 cm^{-1} bands, which correspond to the concentration of methylated aromatics and methoxy species, as a function of the reaction temperature.

These are not the final page numbers! ↗↗

More precisely, the band located at $\lambda \approx 295$ nm grows in intensity, most likely from light olefins produced and trapped on the catalyst owing to the low diffusion properties of the material at this stage.[16,22,24] In addition, the band at $\lambda \approx 410$ nm continues to increase in intensity during the deactivation period while the band at $\lambda = 345$ nm starts to disappear, which also suggests that the $\lambda = 345$ nm band most likely originates from the reaction intermediates in olefin production. Furthermore, the band at $\lambda = 600$ nm assigned to PA species grows during the whole reaction period of the material until reaching a maximum when the catalyst is fully deactivated at 653 K, which implies that the formation of this highly conjugated species may play an important role in the deactivation of the catalyst, more specifically by gradually reducing the accessibility properties of the material until complete blockage. This is in agreement with other lines of thought in which deactivation is attributed to the formation of PA species inside the microporous structure of the material.[25] The origin of the deactivating species, such as PA carbocations, is suggested to be mainly from the reactions involving methanol instead of products.[2] A theoretical modeling study suggested that the side-chain methylation of active hydrocarbon pool species might be a deactivating route leading to coke precursors rather than olefin production.[26]

From the operando IR spectra, depicted in Figure 3b, one can see several changes with respect to the spectra taken during the induction period. In the OH stretching region, there is a red shift in the band with increasing time on stream, which could owe either to an interaction of the acid sites with the hydrocarbons created in the catalyst or to a change in the properties of the acid sites during the course of the reaction. Surprisingly, despite the fact that protonated methyl benzenes were observed by UV/Vis spectroscopy, no characteristic signatures of those species were observed in the CH stretching/bending and C=C stretching regions of the spectrum. This could owe to the low concentration of such species. Above 623 K, changes in the shape of the CH stretching region are observed and signatures ascribed to methoxy species are progressively eroded. Then, a new group of bands appears, with a very intense absorption band at 2925 cm^{-1}. This can be ascribed to CH stretching modes of methyl groups on PA species as suggested previously[27] and in agreement with the UV/Vis data. More indications of the formation of highly conjugated aromatics can be obtained from the $\tilde{\nu} = 1700$–1400 cm^{-1} region, in which two new contributions from C=C stretching modes appear at $\tilde{\nu} = 1600$ and 1580 cm^{-1},[16,28] in addition to the band at $\tilde{\nu} = 1380$ cm^{-1} ascribed to CH bending modes from methyl groups on aromatics.[29]

One of the intriguing questions in the MTO chemistry is the role of the methoxy species in the reaction. Aiming for a better understanding of the function of such species, we investigate whether the depletion of methoxy species is linked to the formation of methylated aromatics. By plotting the integrated area of the $\tilde{\nu} = 940$ and 1380 cm^{-1} band in the IR spectra with the reaction temperature, the methoxy species and alkyl aromatics can be monitored, respectively. This plot is presented in Figure 3c; during the induction period only the for-

mation of methoxy species is observed. Interestingly, during the reaction period the depletion of the methoxy species matches nicely with the formation of alkyl aromatics, suggesting a relationship between them. To corroborate our finding and rule out an effect of the temperature in the desorption and/or depletion of the methoxy species, isothermal reactions were run at different temperatures. The corresponding areas of the $\tilde{\nu} = 940$ and 1380 cm^{-1} bands are plotted in Figure S2. These results clearly confirm our analysis, namely that a decrease in the amount of methoxy species can be related to an increase in the formation of alkyl aromatics.

The results in Figures 3c and S2 can be explained by a blockage of or decrease in the accessibility of the zeotype cavities by the alkylated PA species and a consequent decrease in the formation of methoxy species. Once the methoxy species are completely depleted, at approximately 673 K, the catalyst is finally deactivated. These findings point out that the methoxy species might be directly involved in the catalytic process of the formation of methylated aromatics, most likely by the mechanisms described in the literature for the methylation of olefins[21a,30] and aromatics.[31] However, at this stage in our research we are unable to directly link the alkylation of aromatics via methoxy species and further investigations are needed to substantiate this point. Nevertheless, a direct link between the accessibility of the material and the amount of methoxy species can be made.

We now draw our attention to the last stage of the reaction in which the catalyst wafer is fully deactivated. We observed changes in the UV/Vis operando spectra, displayed in Figure 4a, with temperature even though the catalyst is not active for olefin production in the MTO reaction. Particularly, the absorption band at $\lambda = 600$ nm, ascribed to highly methylated PA species, gradually disappears with increasing reaction temperature, whereas the absorption band at $\lambda = 410$ nm appears to increase in intensity. As none of the species can diffuse outwards, these results can be explained by the transformation of the methylated PA species absorbing light at $\lambda = 600$ nm into other species, such as monoaromatics, naphthalenes, and olefins, by cracking reactions at such high temperatures. Formation of the monoaromatics or less-methylated naphthalene species is observed in the increase in intensity of the absorption band at $\lambda = 410$ nm. In addition, the overall absorbance of the UV/Vis region increases after complete deactivation of the catalyst, as can be better observed in the color-coded Figure 1b. The increase in the overall absorbance is ascribed to the formation of highly conjugated aromatic species that are likely unable to fit in the microporous structure of the material and are consequently deposited onto the external surface of the material.[17a] In the operando IR spectra, depicted in Figure 4b, no substantial changes are observed in the OH stretching region. On the contrary, the effect of temperature in the CH stretching region is remarkable at this stage, with a decrease in the overall absorbance in this region if the reaction temperature is higher than 653 K, which suggests a loss in the methylation degree of the aromatic and PA species. Simultaneously, a new band at $\tilde{\nu} = 3015$ cm^{-1} grows in intensity, which is likely due to the ring CH stretching vibration from less-alkylat-

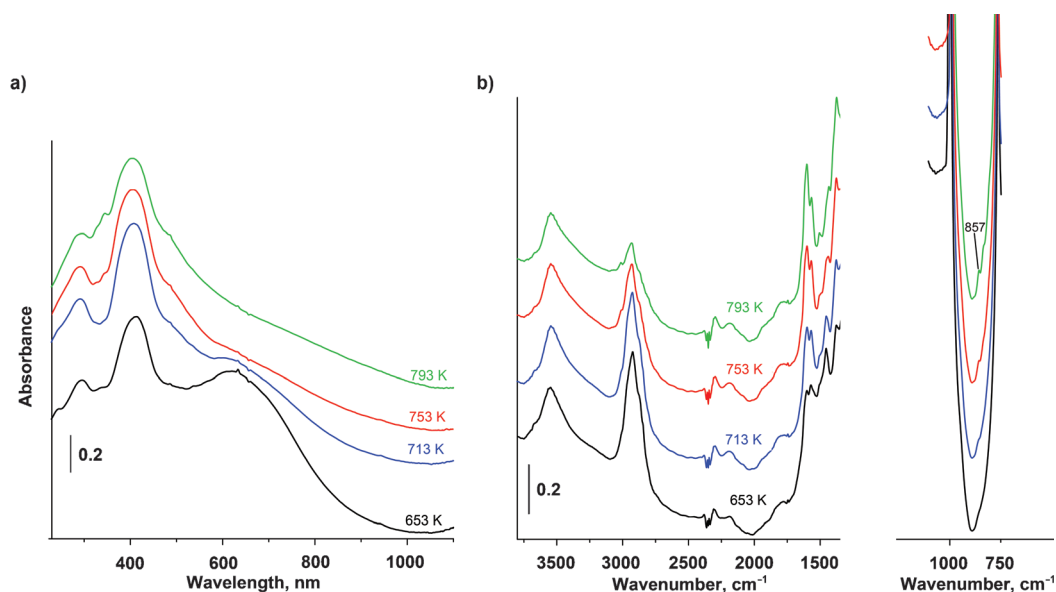**These are not the final page numbers!** ↗↗

Figure 4. Spectroscopic information of the H-SAPO-34 catalyst wafer during the fully deactivated period of the temperature-programmed MTO reaction: a) Operando UV/Vis spectra and b) Operando IR spectra.

ed large aromatics. Diene species are another possible cause of the absorption at $\tilde{v} = 3015$ cm^{-1},[24] which could be formed from dealkylation and/or cracking of PA species. The presence of these less-alkylated large aromatics is confirmed by an increasing intensity in the bands at $\tilde{v} = 1600$ and 1580 cm^{-1}, in combination with the appearance of a band at $\tilde{v} = 857$ cm^{-1} that could owe to the CH out-of-plane bending of the aromatics.[28] Finally, the absence of the band at $\tilde{v} = 940$ cm^{-1} evidences the lack of methoxy species at this stage, which suggests that the material is completely blocked and the changes observed in the spectra are related to the interconversion of the species trapped in the catalyst.

Kinetic studies of catalyst activation and deactivation

Temperature-dependent MTO behavior of SAPO-34

The results in the previous section illustrate that during the MTO reaction the catalytic performance and the nature of hydrocarbon species retained in the H-SAPO-34 material depend critically on the applied temperature. For a more systematic analysis, we have conducted a series of MTO continuous-flow experiments on H-SAPO-34 at reaction temperatures from 508 to 696 K. For each experiment, we applied the same spectroscopic methodology as used in the previous section. Propylene formation during the entire MTO process at different temperatures is displayed in Figure 5a. Two distinct temperature-dependent behaviors can be clearly recognized: in the 508–555 K window, no propylene formation is evidenced and, at higher temperatures, the catalyst is active and produces propylene. This has been confirmed by the analysis of the gas products during the first 2400 s by off-line GC analysis, as shown in Figure 5b. If we inspect the propylene profiles in more detail, the

induction, active, and deactivation periods of the catalyst all become shorter with increasing reaction temperature, which means that the catalyst activates and deactivates faster.

In the next step, we aim to monitor the species that originate in the catalyst upon reaction at different temperatures. Operando IR and UV/Vis spectra of the sample are shown in Figure 5c and d, respectively, before and after the MTO reaction at different temperatures. Initial observation of the IR spectra from the fresh sample shows that this batch of H-SAPO-34 contains slightly more phosphorus hydroxyl groups, which could originate from the calcination procedure. After facilitating the MTO reaction, the Brønsted acid sites are almost eroded at all the temperatures tested, indicating that hydrocarbon species are formed. Further inspection of the IR spectra shows that the formed species have different chemical natures depending on the reaction temperatures, as observed in the C—H stretching region ($\tilde{v} = 2800$–3100 cm^{-1}) and the C=C stretching and C—H deformation region ($\tilde{v} = 1350$–1650 cm^{-1}). At MTO-inert temperatures, the bands at $\tilde{v} = 2975$, 2945, 2845, and 1455 cm^{-1} are indicative of the formation of methoxy and protonated DME species, as discussed in the previous section.[21a,b,27] At MTO-active temperatures, the appearance of a new set of intense bands at $\tilde{v} = 2925$, 1600, 1580, and 1380 cm^{-1} suggests the formation of aromatic species, as discussed above. For a better identification of the aromatic species, UV/Vis spectroscopy is employed because it is more sensitive to the detection of aromatic species, particularly if protonated. On comparing the operando UV/Vis spectra in Figure 5d, it is observed that the absorbance at $\lambda \approx 395$ nm, which is ascribed to PAB carbocations, is much lower in intensity at MTO-inert temperatures. The same trend is observed for the intensity of the band at $\lambda = 600$ nm, which is due to the formation of PA species. Therefore, we can conclude from this set of experi-
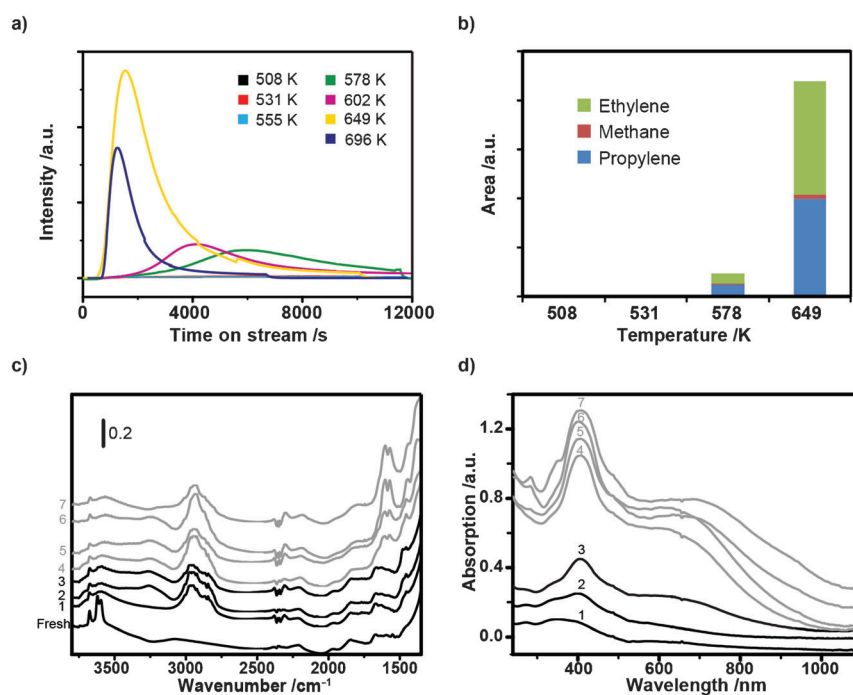
These are not the final page numbers! ⌐⌐

Figure 5. a) Evolution of propylene formation during MTO reactions conducted at different temperatures over the SAPO-34 catalyst monitored by mass spectrometry. b) Off-line GC analysis from the first 2400 s of MTO reactions at the corresponding temperatures. c) Selection of IR spectra taken from the fresh sample and at the end of the MTO reactions conducted at 508 (1), 531 (2), 555 (3), 578 (4), 602 (5), 649 (6) and 696 (7) K. ——: MTO-inert temperatures, ——: MTO-active temperatures. d) Corresponding UV/Vis spectra taken at the end of each MTO reaction.

ments that the extent of production of aromatic species is strongly correlated to MTO performance and the formation of these species depends on the reaction temperature.

The different chemistry of the trapped species was verified by analysis of the retained hydrocarbons by dissolution/extraction experiments after the reaction. The chromatograms of the species extracted, displayed in Figure S3, show very few or no identifiable aromatics at 531 and 555 K, which are inert temperatures. At 578 K, trimethyl and tetramethyl naphthalenes are the most abundant species, followed by hexamethyl benzene and a small amount of trimethyl benzene. At a higher temperature, 693 K, methylated naphthalenes are the predominant species and there is a higher contribution from tetramethyl benzene than from hexamethyl benzene. Additionally, more PA species are observed, such as phenanthrene and pyrene. The results suggest that the UV/Vis band at $\lambda \approx 400$ nm has a significant contribution from naphthalenic carbocationic species, as suggested previously based on molecular dynamic simulations.[32] The assignments of the UV/Vis and IR characteristic bands are summarized in Table S1.

Now, we want to understand the effect of methanol in the evolution of the different hydrocarbon species. For this purpose, we have performed a pulse experiment at 578 K. The UV/Vis spectra and the OH and CO stretching regions in the IR spectra obtained during four consecutive pulses of methanol are displayed in Figure 6. UV/Vis results show that the absorption bands at $\lambda \approx 295$ and 345 nm start to grow during the methanol pulse and decrease in intensity once the pulse is

over. In the IR spectra, methoxy species are formed during the methanol pulse and disappear once the pulse is over, owing most likely to the consumption of these species during the reaction cycle. The changes in the OH stretching region are mostly related to the evolution of methoxy and protonated DME species instead of the formation of aromatic carbocations because the latter cannot diffuse out of the porous systems of SAPO-34.

A more systematic analysis was performed through a deconvolution procedure, in which 10 Gaussian bands were used to properly reconstruct the UV/Vis spectra. As shown in Figure 6d, the three Gaussian bands at $\lambda = 297$, 345, and 450 nm stop growing and even decrease in intensity once the pulse is over. Therefore, the evolution of the species absorbing light at those wavelengths is closely related to methanol. We already know from previous observations that $\lambda = 297$ nm is ascribed to monoenyl carbenium ions, which most probably originate from the transformations of light olefins on the Brønsted acid sites. Additionally, the bands at $\lambda = 345$ and 450 nm are most likely due to di- and trienylic carbenium ions, respectively. Interestingly, the bands at $\lambda = 400$ and 600 nm grow continuously with time on stream, which suggests that the species absorbing light at those wavelengths can be formed from methanol and the interconversion of other species in the catalyst, such as olefins or even the previously mentioned carbocationic species.

Additionally, as shown in Figure 6d, the evolution patterns of methoxy species and propylene are the same, which supports the correlation of the formation of methoxy species with the activity of the material.

Activation energies of activation and deactivation processes

We now aim for a better mechanistic and kinetic understanding of the processes that are active in olefin production (i.e., the activation step) and responsible for deactivation of the catalyst materials (i.e., formation of PA species). As an example, we discuss the reaction conducted at 578 K, a temperature at which the induction and two reaction subperiods (i.e., active and deactivation periods) take place in a time window optimal for the time resolution of our combined spectroscopy approach. The IR and UV/Vis spectra taken from the three abovementioned catalytic stages during MTO at 578 K are displayed in Figure 7. The initial increase in signal intensity observed for
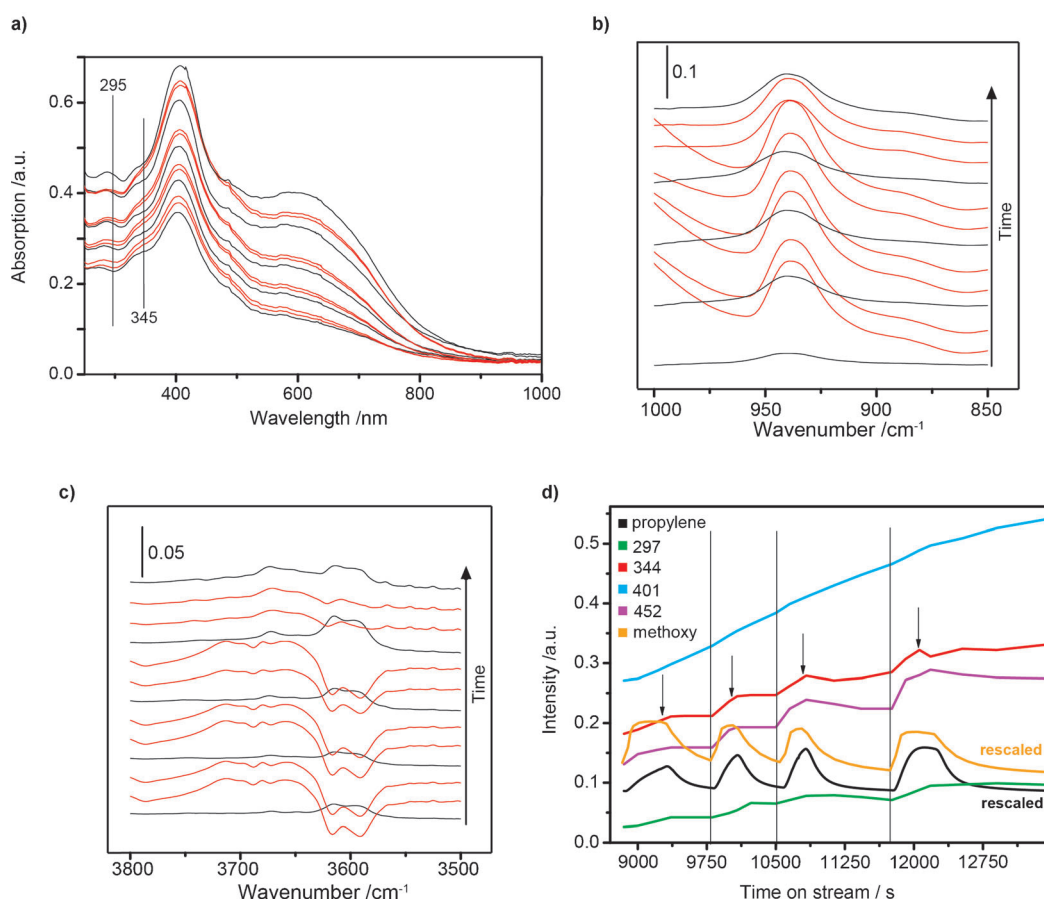
These are not the final page numbers! ↗↗

Figure 6. a) Selection of operando UV/Vis spectra taken during the four-pulse MTO experiment at 578 K. b, c) Selection of operando IR spectra taken at the same time as the operando UV/Vis spectra shown in part a. ——: Spectra taken whilst methanol was in the system, ——: Spectra taken after the methanol pulse. d) Evolution of the $\lambda = 297$, 344, 401, and 452 nm bands of the UV/Vis spectra, the $\tilde{v} = 940$ cm^{-1} band of the IR spectra, ascribed to methoxy species, and the propylene formation during the pulse MTO experiment at 578 K. Black vertical lines and arrows mark the starting and ending points of the methanol pulses, respectively.

propylene in the MS data (at $t < 1000$ s) owes to a stabilization of the signal and therefore no propylene formation is taking place. Propylene formation is indicated by a change in the slope of the signal intensity, as shown in Figure 7 a by a vertical dashed line, and this indicates the transition between the induction and the active period. As the olefin formation drops, the reaction enters the deactivation period. The IR and UV/Vis spectra show distinct signatures during each period, as shown in Figure 7 b–j. During the induction stage, the most important feature is the formation of methoxy species, which is characterized by a CO stretching mode at 940 cm^{-1} and a CH stretching feature at $\tilde{v} = 2978$ cm^{-1} in the IR spectra (Figure 7 b and c). Corresponding UV/Vis results show a weak absorption at $\lambda \approx 395$ nm, which is related to PAB formation (Figure 7 d).

During both active and deactivation periods, spectral similarities can be observed. More specifically, a continuous generation of aromatic species, including both PAB and PA carbocations, is observed, which are characterized by the $\lambda = 395$ and 600 nm bands in the UV/Vis spectra, respectively (Figure 7 g and j). The formation of these aromatics is also reflected in the corresponding IR spectra, as $\tilde{v} = 2925$, 1600 and 1580 cm^{-1} bands increase in intensity and the Brønsted acid site bands

($\tilde{v} = 3625$ and 3595 cm^{-1}) broaden (Figure 7 f and i). These observations suggest that during the two periods of activity and deactivation the chemistry of the aromatic species involved is very similar. If the chemistry of the species is comparable, a change in the accessibility of the material is suggested as the cause of transition from the active period to the deactivation period. This is also reflected in the continuous reduction of methoxy species ($\tilde{v} = 940$ cm^{-1} band) across these two stages (Figure 7 e and h), which, as suggested in the previous section, is due to a blockage of or a decrease in the accessibility of the zeotype cavities by the formation of alkylated PA species.

It is known that methylation reactions on PAB species are essential for the formation of light olefins[33] and PA deactivating species.[26] The intensity of the $\lambda = 600$ nm band as a function of time on stream at different reaction temperatures is shown in Figure 8 a and the derivative curves are shown in Figure 8 b. The derivative curves represent the rate of PA formation at various temperatures. Interestingly, if we compare the rates of propylene (Figure 5 a) and PA (Figure 8 b) formation, the resemblance of these curves is quite clear in terms of shape and intensity at each temperature. This suggests that the olefin pro-
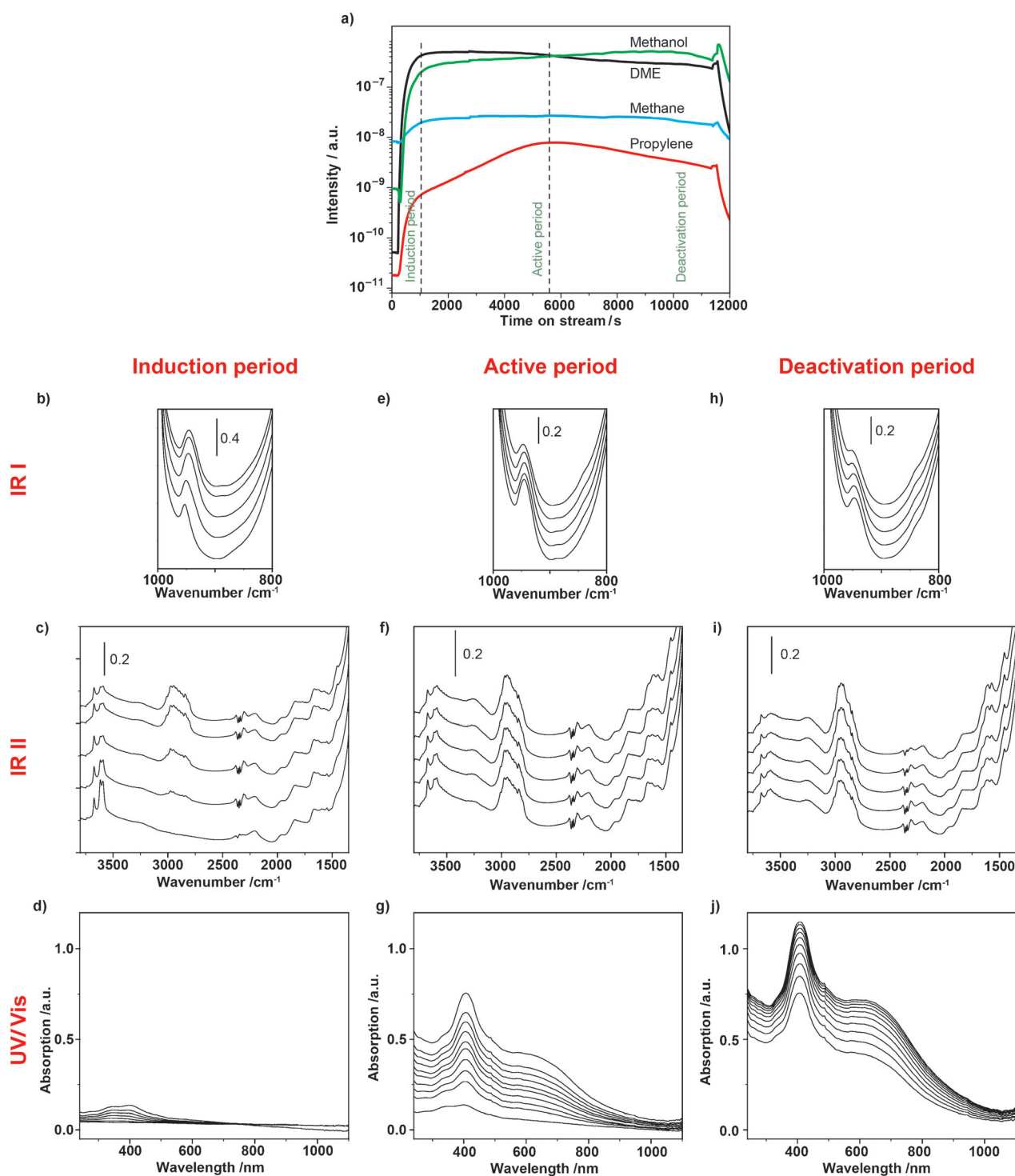
These are not the final page numbers! ↗↗

Figure 7. a) Selection of mass intensity spectra and definition of three reaction periods during the MTO reaction at 578 K. Corresponding IR and UV/Vis spectra taken during the induction (b–d), active (e–g), and deactivation (h–j) periods.

duction (activation step) and PA formation (deactivation step) are two competitive routes based on the same reactants and kinetic models.

If we assume that methoxy species act as the "methylating reagent" and PAB are the species to be methylated, both species will play an equally important role in olefin and PA forma-

tion. Therefore, we propose a kinetic model to describe both reaction steps, which is first order with respect to both methoxy and PAB species. In this model, the formation rates (r) of both olefins and PA species are dependent on the concentration of PAB carbocations ($[PAB^+]$) and methoxy species ($[M]$). For a full description of the model, we refer the reader to the
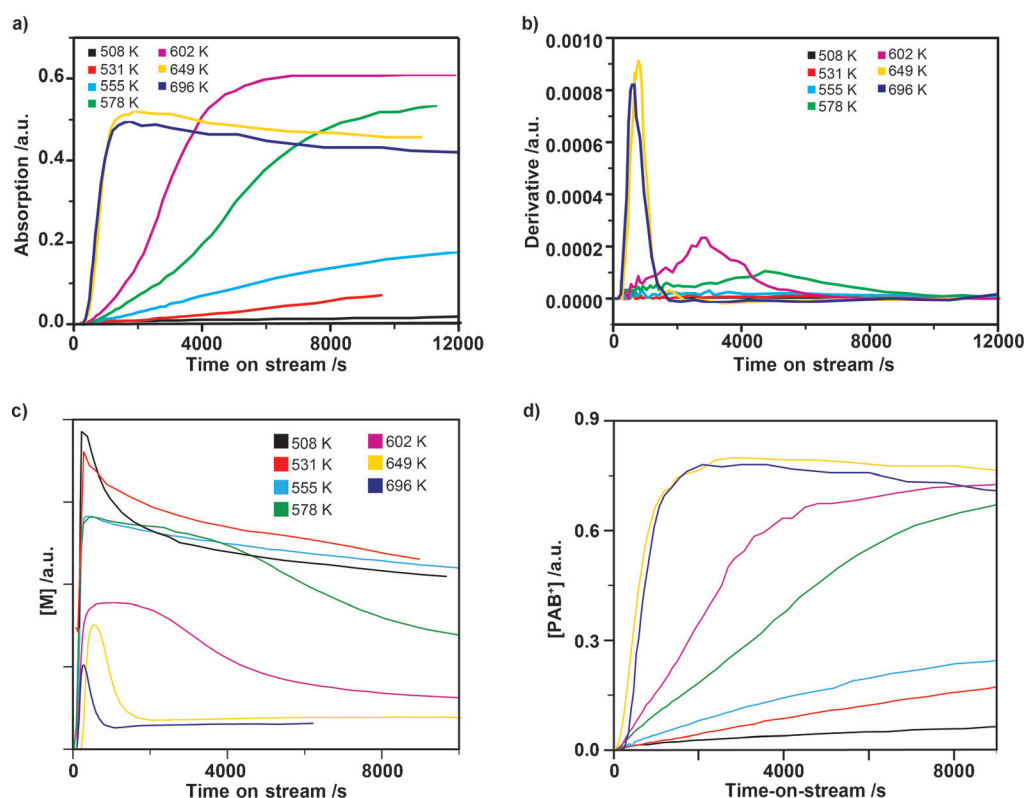
These are not the final page numbers! ↗↗

Figure 8. a) Intensity of the $\lambda = 600$ nm band as a function of time on stream during MTO reactions at different temperatures. b) Derivative curve of the $\lambda = 600$ nm band at different temperatures. c) Concentration of methoxy species integrated from the area of the $\tilde{v} = 940$ cm^{-1} IR band as a function of time on stream during the MTO process at different temperatures. d) Concentration of PAB carbocations deconvoluted from the $\lambda = 395$ nm UV/Vis band as a function of time on stream during the MTO process at different temperatures.

Supplementary Information. For the step of olefin formation, we can deduce Equations (1) and (2), in which k_a represents the rate constant:

$$r_{\text{olefin production}} = k_a \times [M] \times [PAB^+] \tag{1}$$

$$k_a = \frac{r_{\text{olefin production}}}{[M] \times [PAB^+]} \tag{2}$$

For the step of PA formation, similar equations [Eqs. (3) and (4)] can be obtained, in which k_d represents the rate constant:

$$r_{\text{PA formation}} = k_d \times [M] \times [PAB^+] \tag{3}$$

$$k_d = \frac{r_{\text{PA formation}}}{[M] \times [PAB^+]} \tag{4}$$

$$\frac{k_a}{k_d} = \frac{r_{\text{olefin production}}}{r_{\text{PA formation}}} \tag{5}$$

According to Equation (5), a linear relationship exists between the rate of olefins and PA formation during the entire MTO process, which explains the similarity of the curves in Figures 8 b and 5 a, as discussed above. The rate constants can be calculated by monitoring the species involved in the mechanism with time on stream. The amount of PAB carbocations can be monitored by measuring the intensity of the $\lambda = 395$ nm band in the UV/Vis spectra and the amount of me-

thoxy species determined by integrating the band at $\tilde{v} = 940$ cm^{-1} in the IR spectra. The concentration evolutions of methoxy species and PAB carbocations with time-on-stream at each temperature are plotted in Figure 9a and b, respectively. Notably, at MTO-active temperatures (578–696 K), there is a consumption of methoxy species and the amount of PAB carbocations is relatively high.

For the step of PA formation, we can calculate k_d according to Equation (4). The rate of PA formation as a function of [M] and [PAB$^+$] at different reaction temperatures is plotted in Figure 9a. The data points of curves 1 and 2 represent the active and deactivation periods, respectively. It can be seen that the active period follows a linear trend, which suggests that it adheres to the proposed kinetic model. However, this model does not fully agree with observations of the deactivation period, which does not follow a linear trend.

This discrepancy leads us to make some modifications in the kinetic model. If we inspect the active period carefully, for which the proposed kinetic model works, the concentration of methoxy species remains almost constant. Therefore, we can consider the reaction to be of zero order with respect to methoxy species during this stage. Then, the rate Equation (4) can be rewritten for the active period (i.e., curve 1 of Figure 9a) as shown in Equation (6):

$$r_{\text{PA, active period}} = k_d \times [PAB^+] \tag{6}$$
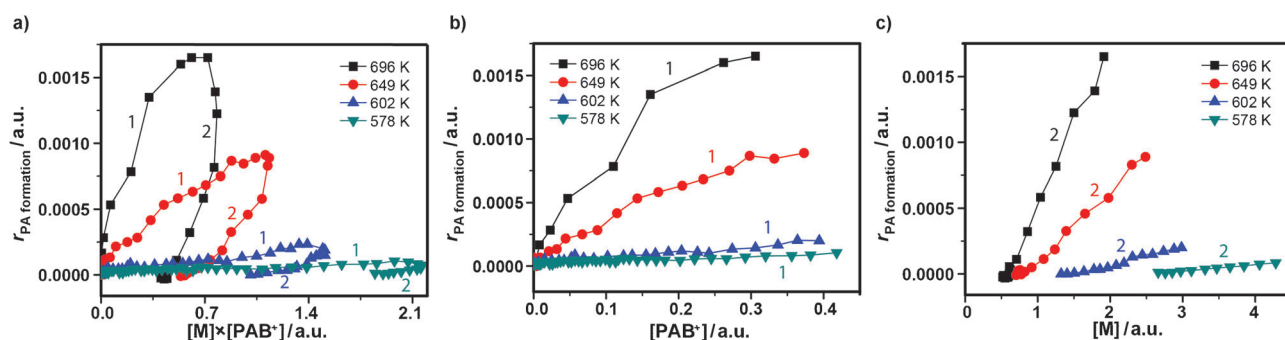
These are not the final page numbers! ↗↗

Figure 9. a) Formation rate of PA as a function of $[M] \times [PAB^+]$ at different active temperatures for MTO reactions. Curves 1 and 2 represent the active and deactivation periods, respectively. b) Formation rate of PA species as a function of the amount of PAB carbocations during the active period of MTO reactions. c) Formation rate of PA species as a function of the amount of methoxy species during the deactivation period of MTO reactions.

Accordingly, the rate of PA formation as a function of PAB concentration is plotted in Figure 9b. As suggested above, it still follows a linear relationship, which indicates that the formation rate of PA species only depends on the concentration of PAB carbocations during the active period. By the same reasoning, we can propose Equation (7) for the deactivation period, in which the reaction appears to be first order with respect to the methoxy species and zero order with respect to the PAB carbocations:

$$r_{PA, \text{deactivation}} = k_d \times [M] \qquad (7)$$

By plotting the rate of PA formation as a function of the methoxy species, a linear relationship exists at all temperatures tested, suggesting that the first-order reaction kinetics applies for these temperatures. However, these linear plots do not go through the origin point of the coordinates, which implies that not all the methoxy species participate in the MTO reaction throughout the whole MTO process. Interestingly, the amount of these inert methoxy species decreases with increasing temperature.

It can be observed that for all the MTO-active temperatures (578–696 K), the formation rate of PA species is first order with respect to the PAB carbocations during the active period but first order with respect to the methoxy species during the deactivation period. Therefore, we can calculate the rate constant k_d at different reaction temperatures by calculating the slopes of curve 1 during the active period (Figure 9b) or those of curve 2 during the deactivation period (Figure 9c). However, the significant pore blockage encountered in the deactivation period forces us to consider that the reaction is controlled by diffusion at this stage. Thus, for a more reliable calculation, k_d values are obtained only from the slopes of curve 1 during the active period, when the reaction is under kinetic control.

For the step of olefin formation, in principle, we can apply the same analytical methodology as for the PA formation. However, the large dead volume of our in situ cell causes a delay in and broadening of the signal attributed to propylene. Consequently, the spectroscopic and MS information are not fully synchronized, although the time difference between the maximum formation rate of PA and that of olefins is quite similar for all the MTO-active temperatures. To make a relatively

accurate calculation of the rate constants at different temperatures, we have taken the maximum intensity of each olefin signal from Figure 5a and calculated the k_a values based on Equation (5) by using the maximum formation rate of PA species measured from Figure 8b and k_d values calculated from Figure 9b.

With these rate constants, we are able to calculate the activation energies (E_a) for both steps of PA formation and olefin formation. The Arrhenius plots for these two steps are shown in Figure S4. The E_a value can thus be calculated from the slope of each linear-fitted curve. However, the linear relationship of the olefin formation (Figure S4b) is not as strong as that for PA formation (Figure S3a), which might owe to the fact that a small amount of olefins may participate in secondary reactions at the time when pore blockage starts to occur. As calculated from the slope of each Arrhenius plot, the E_a value for PA formation and olefin formation is 103 and 97 kJ mol^{-1}, respectively.

Based on the above results, it can be concluded that the two co-existing processes of PA formation and olefin formation, which are also two competitive routes based on the same reactants and kinetic models, have comparable activation energies. We can directly link the information collected by our combined operando spectroscopic approach with the activation route of the catalyst by the formation of olefins and the deactivation route of the catalyst by formation of PA species. Thus, a correlation between the hydrocarbon species inside the SAPO-34 and the catalytic performance can be established. The two reaction cycles for the formation of olefins and PA species are summarized in Scheme 1 in more detail, based on our chemical and kinetic findings from the MTO process. Polymethylated benzenes in both neutral and cationic forms are considered reactants for both cycles. Methoxy species are very likely the methylation agents; furthermore, they are indicators of pore accessibilities. The species shown in black boxes in Scheme 1 are suggested as possible intermediates for both PA and olefin formation.

Conclusions

A combination of operando UV/Vis and IR spectroscopy and on-line mass spectrometry has been used for the first time to

These are not the final page numbers! ↗↗
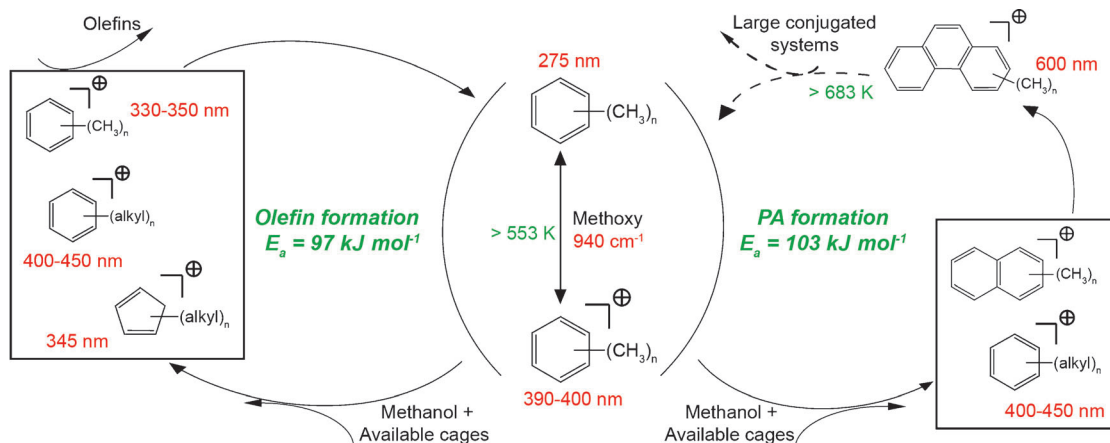
Scheme 1. Reaction cycles for the formation of olefins and PA species with their corresponding activation energies.

monitor the hydrocarbon species formed on a SAPO-34 catalyst during the different stages of the methanol-to-olefins (MTO) reaction under realistic conditions. During the induction period, the major species encountered in the catalyst were methanol, methoxy, and protonated dimethyl ether. A more complex chemistry was observed during the reaction stage of the catalyst and, in addition to the methoxy species, polyalkylated benzene carbocations and PA carbocations species were encountered in the reaction stage of the catalyst. A clear link was found between the accessibility of the zeolite material and the amount of methoxy species. Formation of PA species that absorb light at $\lambda = 600$ nm and plug the microporosity of the material was postulated as the main cause of deactivation of the material. An increase in the reaction temperature after catalyst deactivation accelerated the dealkylation and cracking reactions and the formation of the PA species.

A detailed mechanistic study of the activation (i.e., olefin production) and deactivation (i.e., PA formation) steps was performed. Based on the catalytic and spectroscopic results, it can be concluded that these two steps co-exist and compete through the whole reaction period at MTO-active temperatures (>555 K). Reaction kinetics are proposed to describe both steps during the whole reaction period, which are first-order with respect to the polyalkylated benzene carbocations in the active period and first-order with respect to the methoxy species in the deactivation period. It has been found that the processes leading to olefins and PA species have comparable E_a values of 97 and 103 $kJ\,mol^{-1}$, respectively. As a result, our multi-technique operando approach has allowed us to establish a direct link between the catalytic performance and/or catalyst deactivation and the amount of PA species formed.

Experimental Section

Catalytic material

The SAPO-34 material under study had crystal sizes ranging from 200 to 800 nm and a Si/(Si+Al+P) ratio of 0.037. The template of the as-synthesized SAPO-34 was removed by calcination with the

following procedure: heating at a rate of 2 $K\,min^{-1}$ to 523 K, maintaining the material at this temperature for 3 h, then heating up to 873 K at a rate of 1 $K\,min^{-1}$ in a quartz tubular oven (Thermoline 79300). Subsequently, the sample was ion-exchanged with a 10 wt% NH_4NO_3 solution (Acros Organic, 99+%) 3 times at 343 K.

Analysis of the retained hydrocarbons by dissolution–extraction experiments

The compositions of the retained hydrocarbons in the catalyst materials after MTO reaction were analyzed by using GC–MS. The spent catalyst (15 mg) was transferred to a Teflon tube and dissolved in 48% HF (1.0 cm^3) over 30 min. After that, CH_2Cl_2 (1.0 cm^3) was added to the Teflon tube and the mixture shaken for 30 min. The aqueous and organic phases were left to separate for 30 min. The extraction was repeated 3 times. An aliquot (1 μL) of the resulting organic solution was analyzed on a GCMS-QP2010 device (Shimadzu) connected to a MS detector.

Combined UV/Vis/IR spectroscopy–mass spectrometry

Operando UV/Vis spectroscopy measurements were performed by using an Avantes Avalight-DH-S-BAL probe connected to an Avantes Avaspec 2048L spectrometer. Spectra were recorded every 15 s during each MTO experiment. The corresponding operando IR spectroscopy measurements were performed by using a Bruker Tensor 27 spectrometer coupled with a HgCdTe detector and spectra were taken every 30 s. Additionally, product analysis was performed on a Pfeiffer Vacuum Omnistar mass spectrometer. More specifically, the evolution of methanol, DME, propylene, and methane was followed by monitoring the mass signals 31, 45, 41, and 16, respectively. As displayed in Figure 1, the experimental set-up consisted of an in situ cell with KBr windows where the gas was flown over the catalyst material as a self-supported wafer. UV/Vis measurements were collected in the reflection mode by using a probe with six optical fibers for illumination and one optical fiber for collection. The IR data were measured in transmission and collected by a HgCdTe detector at the same spot on which the UV/Vis probe was focused. Activity data were calculated by identification of the products through gas outlet analysis by using MS. For each MTO reaction, a SAPO-34 catalyst wafer was placed in the heating

These are not the final page numbers! ↗↗

stage of a Linkam FTIR600 cell, which was attached to a Linkam TMS 94 temperature controller. Prior to the MTO reaction, the calcined catalyst was first heated to 473 K at a rate of 5 K min^{-1} and held at this temperature for 10 min, then heated to 773 K at a rate of 10 K min^{-1} and held at this temperature for 1 h in an O_2 atmosphere. Subsequently, the temperature was brought to the required reaction temperature at a rate of 15 K min^{-1}, after which a constant N_2 flow (10 mL min^{-1}) was introduced to a methanol solution and acted as the carrier gas. For temperature-programmed MTO experiments, the temperature was brought from 393 to 823 K at a rate of 4 K min^{-1}. For methanol pulse experiments, each pulse lasted 3 or 6 min and was carried by a N_2 flow of 50 mL min^{-1}. In addition, several temperature-constant MTO experiments were conducted in the temperature region of 500–700 K.

Acknowledgements

Keywords: alcohols · alkenes · in situ analysis · kinetics · zeolites

[1] C. N. Hamelinck, A. P. C. Faaij, *J. Power Sources* **2002**, *111*, 1–22.

[2] M. Stöcker, *Microporous Mesoporous Mater.* **1999**, *29*, 3–48; U. Olsbye, S. Svelle, M. Bjørgen, P. Beato, T. V. W. Janssens, F. Joensen, S. Bordiga, K. P. Lillerud, *Angew. Chem. Int. Ed.* **2012**, *51*, 5810–5831; *Angew. Chem.* **2012**, *124*, 5910–5933.

[3] C. D. Chang, A. J. Silvestri, *J. Catal.* **1977**, *47*, 249–259.

[4] B. Arstad, S. Kolboe, *J. Am. Chem. Soc.* **2001**, *123*, 8137–8138; B. Arstad, S. Kolboe, *Catal. Lett.* **2001**, *71*, 209–212; W. Song, J. F. Haw, J. B. Nicholas, C. S. Heneghan, *J. Am. Chem. Soc.* **2000**, *122*, 10726–10727.

[5] K. Hemelsoet, J. Van Der Mynsbrugge, K. De Wispelaere, M. Waroquier, V. Van Speybroeck, *ChemPhysChem* **2013**, *14*, 1526–1545.

[6] D. M. Marcus, K. A. McLachlan, M. A. Wildman, J. O. Ehresmann, P. W. Kletnieks, J. F. Haw, *Angew. Chem. Int. Ed.* **2006**, *45*, 3133–3136; *Angew. Chem.* **2006**, *118*, 3205–3208; I. M. Dahl, S. Kolboe, *J. Catal.* **1994**, *149*, 458–464; I. M. Dahl, S. Kolboe, *J. Catal.* **1996**, *161*, 304–309.

[7] S. Svelle, U. Olsbye, K. P. Lillerud, S. Kolboe, M. Bjørgen, *J. Am. Chem. Soc.* **2006**, *128*, 5618–5619; M. Bjørgen, S. Svelle, F. Joensen, J. Nerlov, S. Kolboe, F. Bonino, L. Palumbo, S. Bordiga, U. Olsbye, *J. Catal.* **2007**, *249*, 195–207.

[8] S. Svelle, M. Bjørgen, S. Kolboe, D. Kuck, M. Letzel, U. Olsbye, O. Sekiguchi, E. Uggerud, *Catal. Lett.* **2006**, *109*, 25–35; O. Sekiguchi, V. Meyer, M. C. Letzel, D. Kuck, E. Uggerud, *Eur. J. Mass Spectrom.* **2009**, *15*, 167–181.

[9] W. Wang, A. Buchholz, M. Seiler, M. Hunger, *J. Am. Chem. Soc.* **2003**, *125*, 15260–15267.

[10] D. Chen, K. Moljord, T. Fuglerud, A. Holmen, *Microporous Mesoporous Mater.* **1999**, *29*, 191–203; K. Y. Lee, H. J. Chae, S. Y. Jeong, G. Seo, *Appl.* *Catal. A* **2009**, *369*, 60–66; N. Nishiyama, M. Kawaguchi, Y. Hirota, D. Van Vu, Y. Egashira, K. Ueyama, *Appl. Catal. A* **2009**, *362*, 193–199; W. Dai, G. Wu, L. Li, N. Guan, M. Hunger, *ACS Catal.* **2013**, *3*, 588–596; D. Mores, J. Kornatowski, U. Olsbye, B. M. Weckhuysen, *Chem. Eur. J.* **2011**, *17*, 2874–2884; F. Bleken, M. Bjørgen, L. Palumbo, S. Bordiga, S. Svelle, K.-P. Lillerud, U. Olsbye, *Top. Catal.* **2009**, *52*, 218–228.

[11] H. Schulz, *Catal. Today* **2010**, *154*, 183–194.

[12] B. P. C. Hereijgers, F. Bleken, M. H. Nilsen, S. Svelle, K. P. Lillerud, M. Bjørgen, B. M. Weckhuysen, U. Olsbye, *J. Catal.* **2009**, *264*, 77–87.

[13] U. Bentrup, *Chem. Soc. Rev.* **2010**, *39*, 4718–4730.

[14] L. R. Aramburo, J. Ruiz-Martínez, L. Sommer, B. Arstad, R. Buitrago-Sierra, A. Sepúlveda-Escribano, H. W. Zandbergen, U. Olsbye, F. M. F. de Groot, B. M. Weckhuysen, *ChemCatChem* **2013**, *5*, 1386–1394.

[15] M. Bjørgen, F. Bonino, S. Kolboe, K.-P. Lillerud, A. Zecchina, S. Bordiga, *J. Am. Chem. Soc.* **2003**, *125*, 15863–15868.

[16] I. Kiricsi, H. Förster, G. Tasi, J. B. Nagy, *Chem. Rev.* **1999**, *99*, 2085–2114.

[17] D. Mores, E. Stavitski, M. H. F. Kox, J. Kornatowski, U. Olsbye, B. M. Weckhuysen, *Chem. Eur. J.* **2008**, *14*, 11320–11327; D. M. McCann, D. Lesthaeghe, P. W. Kletnieks, D. R. Guenther, M. J. Hayman, V. Van Speybroeck, M. Waroquier, J. F. Haw, *Angew. Chem. Int. Ed.* **2008**, *47*, 5179–5182; *Angew. Chem.* **2008**, *120*, 5257–5260.

[18] J. F. Haw, W. Song, D. M. Marcus, J. B. Nicholas, *Acc. Chem. Res.* **2003**, *36*, 317–326.

[19] L. Smith, A. K. Cheetham, L. Marchese, J. M. Thomas, P. A. Wright, J. Chen, E. Gianotti, *Catal. Lett.* **1996**, *41*, 13–16; B. Zibrowius, E. Löffler, M. Hunger, *Zeolites* **1992**, *12*, 167–174; K. Hemelsoet, A. Ghysels, D. Mores, K. De Wispelaere, V. Van Speybroeck, B. M. Weckhuysen, M. Waroquier, *Catal. Today* **2011**, *177*, 12–24.

[20] S. Bordiga, L. Regli, C. Lamberti, A. Zecchina, M. Bjørgen, K. P. Lillerud, *J. Phys. Chem. B* **2005**, *109*, 7724–7732.

[21] H. Yamazaki, H. Shima, H. Imai, T. Yokoi, T. Tatsumi, J. N. Kondo, *Angew. Chem. Int. Ed.* **2011**, *50*, 1853–1856; *Angew. Chem.* **2011**, *123*, 1893–1896; T. R. Forester, R. F. Howe, *J. Am. Chem. Soc.* **1987**, *109*, 5076–5082; H. Yamazaki, H. Shima, H. Imai, T. Yokoi, T. Tatsumi, J. N. Kondo, *J. Phys. Chem. C* **2012**, *116*, 24091–24097.

[22] H. Förster, S. Franke, J. Seebode, *J. Chem. Soc. Faraday Trans. 1* **1983**, *79*, 373–382.

[23] V. Van Speybroeck, K. Hemelsoet, K. De Wispelaere, Q. Qian, J. Van der Mynsbrugge, B. De Sterck, B. M. Weckhuysen, M. Waroquier, *ChemCatChem* **2013**, *5*, 173–184.

[24] W. Dai, X. Wang, G. Wu, L. Li, N. Guan, M. Hunger, *ChemCatChem* **2012**, *4*, 1428–1435.

[25] D. Chen, H. P. Rebo, K. Moljord, A. Holmen, *Ind. Eng. Chem. Res.* **1997**, *36*, 3473–3479; A. T. Aguayo, A. E. Sánchez Del Campo, A. G. Gayubo, A. Tarrío, J. Bilbao, *J. Chem. Technol. Biotechnol.* **1999**, *74*, 315–321.

[26] D. Lesthaeghe, A. Horré, M. Waroquier, G. B. Marin, V. Van Speybroeck, *Chem. Eur. J.* **2009**, *15*, 10803–10808.

[27] Q. Qian, J. Ruiz-Martínez, M. Mokhtar, A. M. Asiri, S. A. Al-Thabaiti, S. N. Basahel, B. M. Weckhuysen, *ChemCatChem* **2014**, *6*, 772–783.

[28] G. Socrates, *Infrared and Raman Characteristic Group Frequencies: Tables and Charts, 3rd ed.*, Wiley, Chichester, **2001**.

[29] J. W. Park, G. Seo, *Appl. Catal. A* **2009**, *356*, 180–188.

[30] I. M. Hill, S. A. Hashimi, A. Bhan, *J. Catal.* **2012**, *285*, 115–123.

[31] Saepurahman, M. Visur, U. Olsbye, M. Bjørgen, S. Svelle, *Top. Catal.* **2011**, *54*, 1293–1301; S. Svelle, M. Visur, U. Olsbye, Saepurahman, M. Bjørgen, *Top. Catal.* **2011**, *54*, 897–906.

[32] K. Hemelsoet, Q. Qian, T. De Meyer, K. De Wispelaere, B. De Sterck, B. M. Weckhuysen, M. Waroquier, V. Van Speybroeck, *Chem. Eur. J.* **2013**, *19*, 16595–16606.

[33] Q. Qian, J. Ruiz-Martínez, M. Mokhtar, A. M. Asiri, S. A. Al-Thabaiti, S. N. Basahel, H. E. van der Bij, J. Kornatowski, B. M. Weckhuysen, *Chem. Eur. J.* **2013**, *19*, 11204–11215; M. Bjørgen, S. Akyalcin, U. Olsbye, S. Benard, S. Kolboe, S. Svelle, *J. Catal.* **2010**, *275*, 170–180; M. Bjørgen, U. Olsbye, D. Petersen, S. Kolboe, *J. Catal.* **2004**, *221*, 1–10.

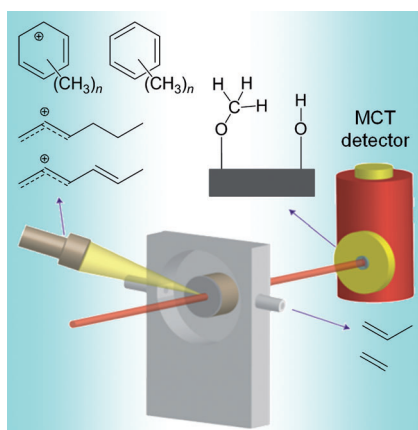**These are not the final page numbers!** ↗↗

FULL PAPERS

Q. Qian, C. Vogt, M. Mokhtar, A. M. Asiri,
S. A. Al-Thabaiti, S. N. Basahel,
J. Ruiz-Martínez,* B. M. Weckhuysen*

■■ – ■■

Combined Operando UV/Vis/IR Spectroscopy Reveals the Role of Methoxy and Aromatic Species during the Methanol-to-Olefins Reaction over H-SAPO-34

Phantom of the operando: During the methanol-to-olefins process over H-SAPO-34 the reaction pathways leading to the formation of olefins and polyaromatics compete. Based on a unique combined operando approach, a first-order kinetic model is proposed to describe both reactions, revealing comparable activation energies. MCT = Mercury–cadmium–telluride.